Journal of Sound and Vibration 576 (2024) 118298

Contents lists available at ScienceDirect

Journal of Sound and Vibration

journal homepage: www.elsevier.com/locate/jsvi

Underwater noise from vibratory pile driving with non-linear frictional pile–soil interaction

Timo Molenkamp *, Athanasios Tsetas, Apostolos Tsouvalas, Andrei Metrikine

Faculty of Civil Engineering and Geosciences, Delft University of Technology, Stevinweg 1, Delft, 2628 CN, The Netherlands

ARTICLE INFO

Keywords:
Underwater noise
Vibratory pile driving
Driveability analysis
Friction
Offshore wind

ABSTRACT

Vibratory offshore pile driving offers a potential solution for reducing the underwater noise generated during the installation of foundation piles compared to using impact hammers. Existing noise prediction models are specifically tailored to impact pile driving scenarios. This paper introduces a novel methodology for underwater noise predictions during vibratory pile driving. A non-linear driveability model is utilised to derive realistic non-linear interface friction forces, which are then incorporated into a noise prediction model. The study emphasises the significance of integrating a driveability analysis, revealing substantial differences from traditional models that assume perfect contact between the pile and soil. The authors argue that the proposed model provides more realistic outcomes when considering smooth driving without refusal, in contrast to traditional models designed for impact piling. The results illustrate noticeable deviations in pressure levels and seabed vibrations between the linear and presented methods at the driving frequency and its superharmonics. Furthermore, the research demonstrates that the noise field is highly sensitive to variations in system dynamics and excitation spectrum during driving, using both small- and large-diameter monopiles as examples. This research contributes to developing more effective driving techniques to reduce underwater noise pollution and facilitate sustainable offshore wind turbine installations.

1. Introduction

Offshore wind has great potential to contribute to European energy. The European Green Deal communication aims to multiply offshore renewable energy almost thirty times while minimising environmental impacts [1]. Currently, most commercial offshore wind projects are bottom-founded wind turbines. The most applied foundation concept is the monopile, a hollow cylindrical pile driven in the soil whose length and diameter range up to 100 m and 10 m, respectively [2].

Impact pile driving is the standard installation technique for monopiles, which causes potential harm and behavioural disturbance to aquatic life [3,4]. Southall et al. [5] confirm this potential harm and publish updated scientific recommendations, stating that even life is at stake for underwater fauna within a few hundred metres of the driving site. Benhemma-Le Gall et al. [6] observed significant porpoise behavioural changes at distances up to 12 km from pile driving sites. These observations underline the importance of accurate noise prediction modelling in the design stage of new wind farms.

Early noise prediction models for offshore pile driving used an acoustic fluid representation of the sediment, emphasising the Mach wave radiation into the fluid domain [7–9]. However, to improve accuracy, subsequent semi-analytical models replaced the fluid representation with spring–damper systems, focusing on improving soil dynamic representation [10,11]. An elastic description of the seabed was subsequently introduced, incorporating the Scholte waves, significantly improving noise prediction models and

* Corresponding author.
E-mail address: T.Molenkamp@tudelft.nl (T. Molenkamp).

https://doi.org/10.1016/j.jsv.2024.118298
Received 28 June 2023; Received in revised form 17 December 2023; Accepted 21 January 2024
Available online 26 January 2024

advancing the understanding of the physical mechanism contributing to the noise and the seabed vibrations [12,13]. Recent research integrated a poroelastic description of the seabed aiming to capture seabed vibrations with better precision [14]. Modelling the seabed is crucial in several ways. First, the elastic description of the seabed improves the sound source characterisation, i.e. pile vibrations. Second, it enhances the description of the noise field at more considerable distances. Third, it provides a more realistic prediction of the wave field along the seabed–water interface, which is richly inhabited by marine life.

Underwater noise levels can be reduced in two ways: either at the source or via a noise mitigation system placed on the path to the receiver, such as air bubble curtains [15,16]. Reducing noise emission at the source is achieved by adjusting the installation method, which vibratory methods have a high potential to accomplish. Vibratory hammers are developed for offshore applications [17] and scaled up to drive larger monopiles. Furthermore, a new vibratory technology called 'Gentle Driving of Piles' is developed to increase driving speed and further reduce noise emissions [18].

Limited research has been conducted on underwater noise caused by vibratory pile driving techniques. Tsouvalas and Metrikine [19] predict the wave field emitted by impact-driven and vibratory-driven monopiles with a traditional noise-prediction model for impact piling. They observe that the highest noise levels are just above the seabed; this phenomenon is more substantial in vibratory pile driving due to the energy carried by the Scholte waves. The Scholte waves are even more dominant under low-frequency excitation, consistent with the primary driving frequency in vibratory pile driving (10∼40 Hz). Furthermore, Tsouvalas and Metrikine [19] note that the system is in a quasi-steady state during vibratory pile driving. Dahl et al. [20] show the dominant presence of the superharmonics of the primary driving frequency (14 Hz) governing the underwater noise emission during vibratory driving. The highest sound pressure levels at 207 m are measured at 112 and 144 Hz; these are multiples of the driving frequency of 16 Hz. Frequencies between multiples of the driving frequency do not significantly contribute to noise emission, i.e. the emitted noise spectrum consists of specific toned components, the frequency of which is dictated by the primary excitation frequency, i.e. the driving frequency, and the non-linear pile–soil interaction. To what extent these superharmonics are induced by hammer excitation or non-linear pile–soil interaction through friction is unknown.

Molenkamp et al. [21] show that noise emission predictions are sensitive to pile–soil interaction modelling. The study introduces a model allowing motion between pile and soil to examine the effect of the pile slip relative to the soil in vibratory pile driving. At low frequencies, such as the primary driving frequency of vibratory devices, the Scholte wave can be the dominant noise carrier when the pile and soil are in perfect contact, i.e., there is no sliding. Contrarily, the first natural frequencies of the system are close to the in-vacuo eigenfrequencies of the pile if pile–soil coupling in the vertical direction is almost absent and noise radiation around those frequencies becomes dominant. For cases in between, no perfect contact with some pile slip is allowed; both mechanisms above are triggered. The paper concludes that an improved description of the interface forces is necessary for accurate noise predictions.

Underwater noise generated by vibratory driving strongly depends on the vibrations of the pile, which act as the acoustic source in the application of interest. Pile vibrations depend strongly on excitation force and soil resistance. Accordingly, noise predictions are sensitive to the pile–soil interaction description. All available underwater noise prediction models use linear soil–pile interaction models, among other reasons, to achieve an acceptable computational time and thereby fail to have a correct physical representation of the interaction.

The novelty of the paper lies in predicting underwater noise due to vibratory pile-driving, with an improved, physically correct representation of the pile–soil interaction. The paper shows the complex dynamics that affect noise emission and examines the influence of the pile–soil interaction. Thus, the underwater noise predictions include non-linear pile–soil frictional interaction via Coulomb friction. The authors believe the numerical model provides a better physical representation of the pile–soil–fluid coupled system, improving our understanding of noise generation mechanisms during offshore vibratory pile driving. At low frequencies, it is essential to accurately calculate the amplitude of the Scholte interface waves, and at higher frequencies, the pile–soil coupling strongly affects the steady-state response of the system and the energy distribution into the various superharmonics. A non-linear pile driveability analysis provides information on the progression of the pile into the soil and the non-linear interaction forces.

The effect of the non-linear pile–soil interaction is implemented in a vibroacoustic model by utilising the output from a vibratory driving analysis, provided that the driveability model is three-dimensional. Tsetas et al. [22] developed a computationally efficient 3-D axisymmetric pile–soil model for vibratory driving and validated the numerical model predictions with field data. In particular, a linear elastic thin cylindrical shell and a linear elastic layered half-space describe the pile and soil medium, respectively. Their coupling is realised through a history-dependent frictional interface based on Coulomb friction. In that manner, a reliable estimation of the pile–soil interaction forces can be obtained and utilised as input for the subsequent step, namely the underwater noise predictions.

This paper introduces a novel approach by integrating a comprehensive non-linear representation of pile–soil friction into an underwater noise prediction model. In doing so, the knowledge gaps in the field above are closed. The models and their interactions are described in Section 2. The approach is demonstrated via two case studies involving piles of different sizes. The case of a small-size pile refers to the practical application of a pin pile in a jacket structure and is examined in Section 3. The pile dimensions are chosen according to limited available combined data from two experimental campaigns, one onshore and one offshore. Section 4 discusses the case of a large-diameter monopile, referring to a commercial pile foundation for modern applications. While vibratory hammers have not been tested commercially, extrapolated data from small-scale tests is used to perform the underwater noise modelling. The impacts of driving frequency and penetration depth on noise emissions are explored. The research displays that accurate noise predictions during vibratory pile driving are sensitive to the resonances of the system, depending on the pile–soil interaction model. Acoustic pressure underwater depends strongly on the varied driving frequency, force spectrum, and pile penetration depth. The effect of non-linear pile–soil interaction is compared to conventional models, and a theoretical rationale is presented for the noise generation phenomenon. The conclusions are provided in Section 5.

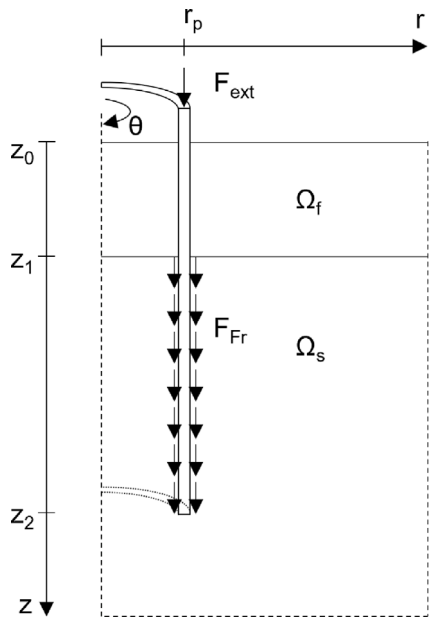

Fig. 1. Model geometry with the acoustic fluid domain Ω_f and the elastic soil domain Ω_s. The pile is modelled by thin-shell theory at $r = r_p$.

2. Methodology

This section introduces a methodology integrating realistic non-linear frictional interface forces into noise prediction analysis. To achieve this, a state-of-the-art driveability model for vibratory pile driving is utilised to simulate the process of pile penetration and generate non-linear friction forces throughout the driving procedure [22]. The friction forces are obtained at discrete pile penetration depths, transformed into the frequency domain, and used as input in the noise prediction model. The proposed noise prediction model [21] employs a boundary integral formulation to describe the fluid–soil domain, enabling the direct incorporation of the friction forces. This section presents the geometrical characteristics and fundamental equations of the proposed model. Subsequently, it briefly overviews both analysis methods and explains how the analyses fit into the methodology.

2.1. Geometrical characteristics and fundamental equations

Fig. 1 visualises the configuration of a monopile installation offshore containing a hollow cylinder driven into the soil. The monopile occupies the domain $z_2 - L_p < z < z_2$, with pile length L_p, thickness h_p and diameter $2r_p$. The problem is cylindrically symmetric, i.e., the cylindrical coordinate system (r, z) is employed, assuming no variation around the circumference.

The pile is modelled as a thin shell, and its modulus of elasticity, Poisson's ratio and pile density are E_p, ν_p, and ρ_p, respectively. The equation of motion of the pile reads:

$$\boldsymbol{L}_p \boldsymbol{u}_p(z,t) + \rho_p h_p \ddot{\boldsymbol{u}}_p(z,t) = \boldsymbol{f}_p(z,t) + f_{ext}(t)\delta(z - z_{top})\hat{\mathbf{e}}_z \tag{1}$$

where $\boldsymbol{L}_p$ represents the stiffness components of Flügge's thin shell theory [23], $\hat{\mathbf{e}}_z$ is the vertical normal vector. The vector of the pile displacements reads $\boldsymbol{u}_p(z,t)$, $f_{ext}(t)$ provides the external load on top of the pile, and $\boldsymbol{f}_p(z,t)$ contains the distributed fluid and soil interaction forces. The overhead double dots refer to the second derivative in time: $\partial^2/\partial t^2$.

The seawater and soil are modelled as continua, occupying the domains $z_0 < z < z_1$ and $z > z_1$, respectively. The first is described as an acoustic fluid, while the latter is modelled as an elastic medium. The fluid wave speed and density are given by c_f and ρ_f, respectively. The soil is characterised by the Lamé constants λ_s and μ_s and density ρ_s. The equations of motion of the domains read:

$$\nabla^2 \phi_f(r,z,t) - \frac{1}{c_f^2}\ddot{\phi}_f(r,z,t) = s_f(z,t)\delta(r - r_p) \tag{2}$$

$$(\lambda_s + \mu_s)\nabla(\nabla \cdot \boldsymbol{u}_s(r,z,t)) + \mu_s \nabla^2 \boldsymbol{u}_s(r,z,t) + \boldsymbol{f}_s(z,t)\delta(r - r_p) = \rho_s \ddot{\boldsymbol{u}}_s(r,z,t) \tag{3}$$

The motion of the acoustic fluid is described by the displacement potential $\phi_f(r,z,t)$, which relates to the displacement field via $\boldsymbol{u}_f(r,z,t) = \nabla\phi_f(r,z,t)$ and the fluid pressure $p_f(r,z,t) = \rho_f \omega^2 \phi_f(r,z,t)$ [24]. The soil equation of motion contains displacements vector $\boldsymbol{u}_s(r,z,t)$ and body loads $\boldsymbol{f}_s(z,t)$ applied at $r = r_p$.

The fluid and soil are coupled through a standard set of interface conditions along the vertical coordinate valid at $r < r_p$ and $r > r_p$:

$$p_f(r, z_1, t) = 0 \tag{4}$$

$$p_f(r, z_2, t) + \sigma_{s,zz}(r, z_2, t) = 0 \tag{5}$$

$$u_{f,z}(r, z_2, t) - u_{s,z}(r, z_2, t) = 0 \tag{6}$$

$$\sigma_{s,zr}(r, z_2, t) = 0 \tag{7}$$

The coupling of the fluid and soil with the pile at $r = r_p$ deviates from the standard linear underwater noise prediction models due to the introduction of friction at the pile–soil interface:

$$u_{p,r}(z, t) = u_{f,r}(r_p, z, t) \qquad z_0 < z < z_1 \tag{8}$$

$$f_{p,r}(z, t) = -p_f(r_p^+, z, t) + p_f(r_p^-, z, t) \qquad z_0 < z < z_1 \tag{9}$$

$$u_{p,r}(z, t) = u_{s,r}(r_p, z, t) \qquad z_1 < z < z_2 \tag{10}$$

$$f_{p,r}(z, t) = \sigma_{s,rr}(r_p^+, z, t) - \sigma_{s,rr}(r_p^-, z, t) \qquad z_1 < z < z_2 \tag{11}$$

$$f_{p,z}(z, t) = F_{Fr}(z, t) \qquad z_1 < z < z_2 \tag{12}$$

$$F_{Fr}(z, t) = -\sigma_{s,rz}(r_p^+, z, t) + \sigma_{s,rz}(r_p^-, z, t) \qquad z_1 < z < z_2 \tag{13}$$

in which the interior and exterior domains are indicated with superscripts '−' and '+', respectively. Eqs. (8) and (9) describe the pile–fluid interaction along the radial direction. Eqs. (10) and (11) prescribe continuity of stresses and displacements between pile and soil in the radial direction. Friction is introduced as $F_{Fr}(z, t)$ in Eqs. (12) and (13) being a distributed vertical force acting on the pile surface while balancing the difference between internal and external shear stresses in the soil. The driveability and noise prediction analyses are run sequentially to resolve the described problem statement as schematised in Fig. 2.

2.2. Driveability analysis

To perform a pile driving analysis, a non-linear pile–soil interaction model is necessary to describe the pile penetration into the seabed. In particular, various modelling developments are ongoing both in impact piling [25,26] and vibratory driving [22,27], focusing on the challenges of offshore monopile installation. Tsetas et al. [22] developed an axisymmetric model for vibratory driving that is comprised of a linear elastic thin cylindrical shell and a linear elastic (layered) half-space. The fluid layer is excluded because its presence does not influence the driveability analysis, a commonly accepted assumption in driveability modelling. Specifically, the pile vibrations are modelled using the Semi-analytical Finite Element (SAFE) method, where the cylindrical shell is discretised into a set of nodal rings. As regards the soil medium, the Thin-Layer Method (TLM) is employed to discretise the layered soil domain into homogeneous horizontal layers of small thickness (in finite element sense) [28]. It is noted that the half-space is accounted for in this model by utilising Perfectly Matched Layers (PMLs) coupled with the TLM [29,30]. Therefore, pile and soil modelling approaches employ a typical vertical discretisation grid. Furthermore, the non-linear pile–soil interaction is realised through a history-dependent frictional interface based on Coulomb friction that captures the progressive friction reduction at the pile–soil interface. The previous is commonly termed friction fatigue in the context of pile driving [31]. Finally, the vibratory pile driving model uses a visco-elasto-plastic tip reaction.

The friction force at $r = r_p$ is expressed as follows:

$$F_{Fr}(z, t) = f_{s,ult}(z, t) \tanh\left(\frac{1}{v_{tol}}\left(\frac{\partial u_{s,z}(r_p, z, t)}{\partial t} - \frac{\partial u_{p,z}(z, t)}{\partial t}\right)\right) \tag{14}$$

where v_{tol} is a velocity tolerance parameter and $f_{s,ult}(z, t)$ defines the amplitude of the static (and kinetic) friction. It is noted that Eq. (14) accounts for the friction forces from both the inner and outer pile surfaces. Furthermore, in the present friction force formulation, the friction amplitude possesses history-dependence that is described as follows:

$$f_{s,ult}(z, t) = f_{s,0}(z)\left(\beta_\infty + (1 - \beta_\infty)e^{-c_N N_{cycl}(z,t)}\right) \tag{15}$$

where β_∞ is the ratio of the ultimately degraded friction amplitude to the initial one $f_{s,0}(z) = 0.012 q_c(z)$, $q_c(z)$ is the cone tip resistance of Cone Penetration Test (CPT), c_N is a memory parameter that controls the rate of degradation and $N_{cycl}(z, t)$ is the number of loading cycles accumulated at the soil position z during driving. Accordingly, as the pile penetrates the ground, the loading cycle accumulation at each soil material point reduces the friction force at the respective point.

The problem of non-linear dynamic pile–soil interaction is resolved by applying the Harmonic Balance Method (HBM) sequentially [32–34]. The HBM is used to determine a solution at each compatible position, where the elevations of the pile nodal rings align with the interfaces of soil layers. This solution remains valid for a time interval, significantly surpassing the fundamental period of the harmonic balance since the pile position and overall response change at a much slower pace compared to the driving frequency. This discrepancy in time scales allows for the sequential determination of harmonic balance coefficients for every pile position along the vertical mesh.

A more elaborate description of the model development, the friction parameters and the associated results can be found in Tsetas et al. [22]; these will be omitted, as the focus herein lies in the underwater acoustics of vibratory pile installation. Further validation of the driveability model with field data regarding penetration rates and pile vibrations can also be found in [35,36].

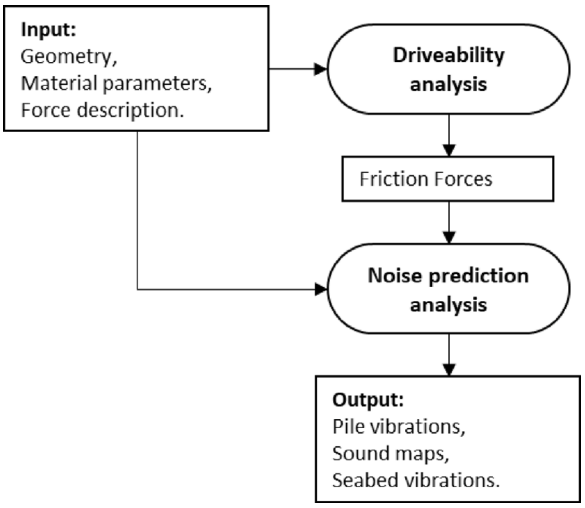

Fig. 2. Flow chart of interaction between the driveability and the underwater noise prediction models.

2.3. Noise prediction analysis

The underwater noise and seabed vibrations induced by vibratory pile driving are obtained via a noise prediction model. The model introduced in Molenkamp et al. [21] allows for relative motion between pile and soil, making it suitable to apply friction forces directly at the pile–soil interface. The governing equations for pile, fluid and soil are introduced in Section 2.1. The method describes the internal and external fluid and soil domains based on boundary integral formulation of ring source Green's functions in the frequency domain. A modal summation of the in-vacuo modes represents the pile vibrations. The frequency domain representation of Eq. (1), including friction forces along the vertical direction and radial fluid and soil resistances, reads:

$$\boldsymbol{L}_{\mathrm{p}}\tilde{\boldsymbol{u}}_{\mathrm{p}}(z,\omega)-\rho_{\mathrm{p}}h_{\mathrm{p}}\omega^{2}\tilde{\boldsymbol{u}}_{\mathrm{p}}(z,\omega)=\tilde{F}_{\mathrm{fsr}}(z,\omega)\hat{\mathbf{e}}_{\mathrm{r}}-\tilde{F}_{\mathrm{Fr}}(z,\omega)\hat{\mathbf{e}}_{\mathrm{z}}+\tilde{f}_{\mathrm{ext}}(\omega)\delta(z-z_{\mathrm{top}})\hat{\mathbf{e}}_{\mathrm{z}} \tag{16}$$

where the tilde refers to the complex amplitude in the frequency domain. F_{fsr} contains the radial fluid and soil responses on the pile; these are found by convolution in z of the ring source Greens functions of the fluid and soil domain and the radial pile displacements and friction forces:

$$\tilde{F}_{\mathrm{fsr}}(z,\omega)=-\int_{z_1}^{z_2}\tilde{\boldsymbol{K}}_{\mathrm{fs}}^{\mathrm{u_{pr}}}(\omega,z,\bar{z})\tilde{u}_{\mathrm{pr}}(\omega,\bar{z})\mathrm{d}\bar{z}+\int_{z_1}^{z_2}\tilde{\boldsymbol{K}}_{\mathrm{fs}}^{\mathrm{F_{Fr}}}(\omega,z,\bar{z})\tilde{F}_{\mathrm{Fr}}(\omega,\bar{z})\mathrm{d}\bar{z} \tag{17}$$

in which $\tilde{\boldsymbol{K}}_{\mathrm{fs}}(\omega,z,\bar{z})$ contains the required Green's functions and Green's tensors of fluid and soil domains. A modal summation represents the pile displacements:

$$\tilde{\boldsymbol{u}}_{\mathrm{p}}(z,\omega)=\sum_{k=1}^{\infty}\tilde{\xi}_{k}(\omega)\boldsymbol{U}_{\mathrm{p},k}(z,\omega) \tag{18}$$

The mode shapes $\boldsymbol{U}_{\mathrm{p},k}(z,\omega)$ are found by solving the eigenvalue problem of the in-vacuo pile with free-end boundary conditions. The modal amplitudes $\tilde{\xi}_{k}(\omega)$ are obtained by applying the orthogonality of the structural modes in Eq. (16):

$$(\omega_{k}^{2}(1+\mathrm{i}\eta_{\mathrm{p}})-\omega^{2})\tilde{N}_{k}(\omega)\tilde{\xi}_{k}(\omega)=\sum_{l}\int_{0}^{z_2}\boldsymbol{U}_{\mathrm{pr},l}^{T}(z,\omega)\tilde{F}_{\mathrm{fsr}}(z,\omega)\mathrm{d}z-\int_{z_1}^{z_2}\boldsymbol{U}_{\mathrm{pz},l}^{T}(z,\omega)\tilde{F}_{\mathrm{Fr}}(z,\omega)\mathrm{d}z+U_{\mathrm{pz},l}(0,\omega)f_{\mathrm{ext}}(\omega) \tag{19}$$

in which η_{p} is the structural damping, only admissible for small values ($\eta_{\mathrm{p}}<10^{-2}$) as no effect of damping on the structural modes is considered, and N_k is the orthogonality condition of the pile modes:

$$\tilde{N}_{k}(\omega)=\rho_{\mathrm{p}}h_{\mathrm{p}}\int_{0}^{L_{\mathrm{p}}}\boldsymbol{U}_{\mathrm{p},k}^{T}(z,\omega)\boldsymbol{U}_{\mathrm{p},k}(z,\omega)\mathrm{d}z \tag{20}$$

The integrals in Eq. (19) and in the convolutions in Eq. (17) are solved by numerical integration. After finding the pile vibrations and having the friction forces, the waves are straightforwardly propagated at larger distances from the pile by employing Green's functions and Green's tensors of ring sources. A more elaborated model description and detailed derivation of Green's functions and Green's Tensors are found in [21].

2.4. Integrating driveability effects in noise prediction analysis

The driveability analysis subsequently provides the non-linear frictional interface forces at each driving depth, described in Eq. (14). The friction forces are consecutively substituted in the noise prediction analysis. Since the driveability model employs

Table 1
Parameters for the small diameter monopile case study [20,37].

Parameter		Unit	Parameter		Unit
Sea surface depth [z_1]	0	m	Fluid wave speed [c_f]	1500	$m\,s^{-1}$
Seabed depth [z_2]	7.5	m	Fluid density [ρ_f]	1000	$kg\,m^{-3}$
Pile length [L_p]	17.4	m	Compression wave speed soil [c_L]	1800	$m\,s^{-1}$
Pile thickness [t_p]	2.54	cm	Shear wave speed soil [c_T]	200	$m\,s^{-1}$
Pile radius [r_p]	0.762	m	Soil density [ρ_s]	1900	$kg\,m^{-3}$
Pile Poisson's ratio [ν_p]	0.28	–	Compressional wave attenuation [α_L]	0.80	dB/λ
Pile Young's modulus [E_p]	210	GPa	Shear wave attenuation [α_T]	0.20	dB/λ
Pile density [ρ_p]	7850	$kg\,m^{-3}$	Cone tip resistance [q_c]	10	MPa
Structural damping [η_p]	0.001	–			

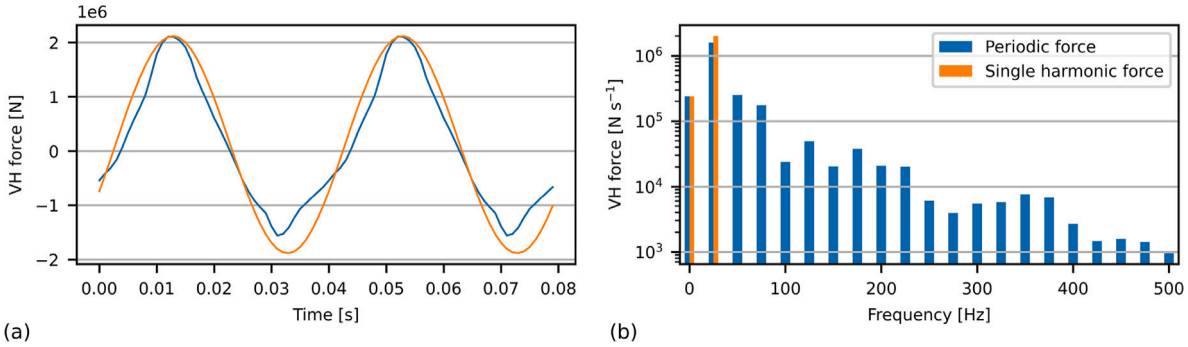

Fig. 3. (a) Two cycles of the single harmonic and periodic force in the time domain and (b) the amplitude per frequency.

the HBM around each driving depth, all forces and displacements are expressed by a summation of harmonics. Thus, the friction forces can straightforwardly be substituted in Eq. (19), the noise prediction analysis, to find the frequency domain pile vibrations, fluid pressures and soil vibrations. The analysis is run in the state of constant driving, excluding refusal, defined as the state where the pile does not progress into the soil.

A significant benefit of combining both methods is the computational efficiency of the independent components. A single analysis, i.e. a single driving force, of the large monopile was executed on an Intel(R) Xeon(R) W-2155 CPU @ 3.30 GHz in 142 min. The driveability analysis took 36 min, generating the soil and fluid BEM 34 min, calculating the fluid and soil propagation matrix 56 min and performing the acoustic frequency domain analysis 16 min. The computation time depends mainly on the number of frequencies, pile and BEM discretisation and the number of receiver points in the soil and fluid. This study does not include further considerations, such as parallel computation optimisation for increased computational speed.

3. Underwater noise field of a small-size monopile

The underwater noise field generated during the driving of a small-scale monopile with a vibratory hammer is examined based on experimental data. The case study consists of a small monopile with a diameter of 0.762 m as used in the experimental campaign of both Tsetas et al. [18] and Dahl et al. [20]. The geometry is taken from Dahl et al. [20], and common values are used for sandy soil and fluid retrieved from Peng et al. [37]. The parameters are outlined in Table 1.

Two external forcing functions are applied to the pile. First, a single harmonic excitation is combined with a static load, referring to a perfect vibratory hammer. Second, a driving force is deduced from measurements during the test campaign of Tsetas et al. [18]; the first is referred to as the single harmonic force and the latter as the periodic force.

A static load is assumed to be 120 kN, and the single harmonic force excites 25 Hz with an amplitude of 2.5 MN. These values result in the same pile penetration rate as the force obtained from the test campaign with the same primary driving frequency. The obtained force from measurements is periodic, with a primary driving frequency of 25 Hz plus excitation at several superharmonics. Accordingly, the force is described by the following Fourier series:

$$f_{\text{ext}}(t) = \sum_{n=0}^{20} c_n e^{i2\pi f_0 n} \tag{21}$$

with f_0 being the primary driving frequency and c_n the complex valued amplitude. The number of superharmonics is truncated to 20, corresponding to 500 Hz since the sampling rate was at one kHz. The Fourier component at $n = 0$ corresponds to the static force on top of the pile. Fig. 3 shows each force's time series and amplitude–frequency spectra. The contributions of the superharmonics in the periodic force obtained from the test campaign are magnitudes smaller than the primary driving frequency and decrease with increasing frequency; the figure justifies that frequencies above 500 Hz are not expected to contribute significantly to the response

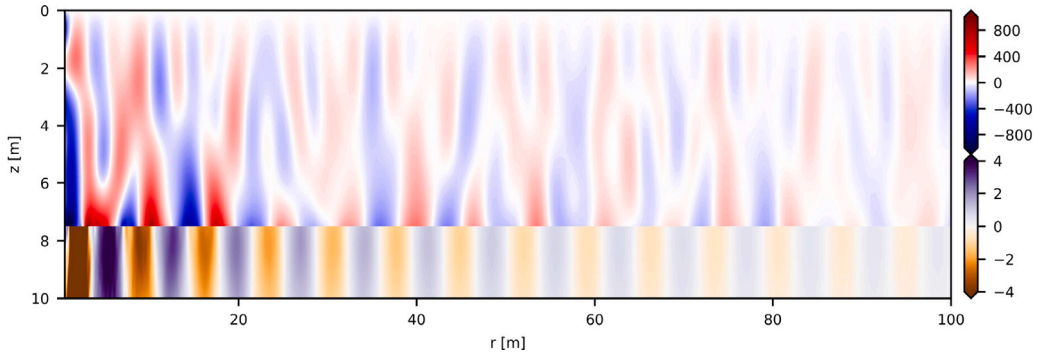

Fig. 4. Snapshot of the underwater pressure and vertical seabed velocity at a driving depth of $z_2 = 14$ m due to a single harmonic force. The blue–red scale shows the fluid pressure in Pa, and the yellow–purple scale shows the vertical soil particle velocity in $\mathrm{mm\,s^{-1}}$. (For interpretation of the references to color in this figure legend, the reader is referred to the web version of this article.)

of the coupled system. The periodic force represents the hammer force on top of the pile based on measurements. However, the real force and corresponding spectrum depend on driving depth, pile size, soil conditions, and hammer type; during this analysis, the spectral distribution of the force is assumed to be constant.

3.1. Single harmonic force

Two wave paths are typically identified in noise generation during offshore pile driving. The primary noise path is considered the direct noise path of the pile radiating noise into the fluid; the secondary noise path contains the noise that is generated indirectly by soil vibrations, e.g. by the Scholte interface wave, i.e. the pile excites the soil, and via seabed vibrations the fluid is excited. Fig. 4 shows the underwater pressure field and seabed vibrations excited by a single harmonic force at a driving depth of $z_2 = 14$ m; this is halfway through the driving process. The primary noise path is visible in the fluid domain, where the fluid is directly excited by the pile vibrations; the second noise path is clearly visible in the soil vibrations but is more difficult to detect in the fluid. Nonetheless, pressure waves propagate just above the seabed with a quarter-period shift from the vertical soil velocity. The phase shifts originate from pressure being proportional to accelerations, and the interface waves have an exponential decay from the seabed into the fluid layer. Observing the primary noise path, there is an interference of multiple waves. However, the dominant wavelength of the body waves is approximately ten m, corresponding to waves with a frequency of 150 Hz, which is not the primary driving frequency. The frictional resistance at the pile–soil interface obtained by the non-linear driveability model is the only mechanism that can redistribute energy in this model from the single harmonic excitation to superharmonics.

Sound pressure levels give insight into the contribution of each frequency to the noise field. The sound pressure levels L_P are calculated via [38]:

$$L_\mathrm{p} = 20 \log \left(\frac{p_\mathrm{rms}}{p_\mathrm{ref}} \right) \tag{22}$$

in which the real mean square in the frequency domain equals $p^2_\mathrm{rms} = \frac{1}{2}|\tilde{p}^2|$ and the reference pressure in underwater acoustics is $p_\mathrm{ref} = 1$ μPa.

Fig. 5 clearly shows that energy shifted to super harmonics and that these higher harmonics govern the noise field. This confirms the significance of combining driveability analysis with noise predictions since linear models cannot predict energy redistribution into higher harmonics that govern the sound radiation.

The sound pressure levels amplify around the natural frequencies of the in-vacuo pile, which are indicated with red dotted vertical lines in Fig. 5. The axisymmetric pile modes have significantly larger vertical than radial deformations at the first few natural frequencies. Consequently, the first few resonant frequencies of the immersed structure shift only slightly from the in-vacuo natural frequencies of the pile since the pile and surrounding media are coupled only strongly in the radial direction when relative vertical motion is allowed between pile and soil [21].

The superharmonics at 150, 300 and 450 Hz almost coincide with the natural frequencies of the in-vacuo pile with free-edge boundary conditions at 149, 297 and 445 Hz, resulting in significant radial vibrations. Consequently, the fluid pressure is governed by the body waves radiated from the pile at these frequencies, even though the hammer force does not directly excite these frequencies. Thus, the sound pressure levels are highest at frequencies excited by frictional resistance, underlining the importance of an accurate pile–soil interface description.

Fig. 5 presents the sound pressure levels at three driving depths of the pile. The sound pressure levels significantly reduce with driving depth at frequencies between 100 and 150 Hz. At other frequencies, the difference is more minor. The sound pressure levels at the primary driving frequency remain largely unaffected by the driving depth. Driving depth significantly affects the dynamic behaviour of the immersed structure, but the effect is not straightforwardly predictable.

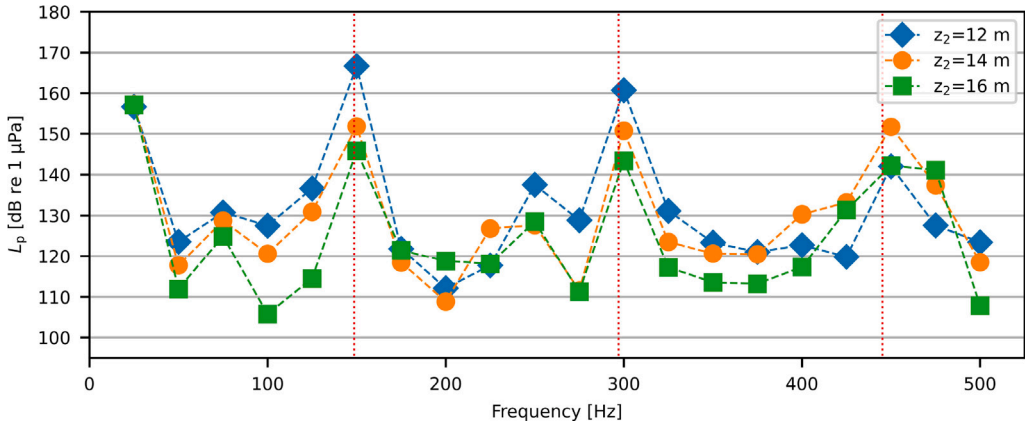

Fig. 5. Sound pressure levels above the seabed at $r = 50$ m and $z = 4$ m for three different driving depths. The red dotted vertical lines represent the pile's first three in-vacuo natural frequencies.

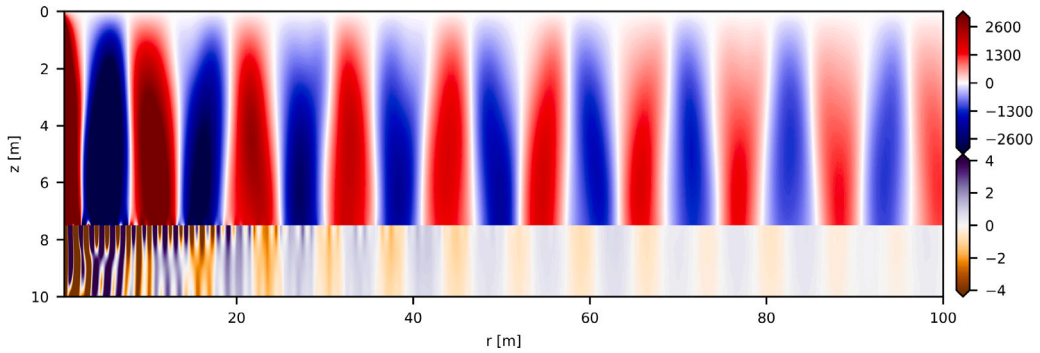

Fig. 6. Snapshot of the underwater pressure and vertical seabed velocity at a driving depth of $z_2 = 14$ m. The blue–red scale shows the fluid pressure in Pa, and the yellow–purple scale shows the vertical soil particle velocity in $\mathrm{mm\,s^{-1}}$. (For interpretation of the references to color in this figure legend, the reader is referred to the web version of this article.)

3.2. Periodic force

A periodic force on top of the pile provides a more realistic case. Fig. 6 shows the underwater pressure field and seabed vibrations at a driving depth of $z_2 = 14$ m. The Body waves with a ten m wavelength, corresponding to a frequency of 150 Hz, dominate the pressure field in the fluid. This aligns with the observed pressure field in Fig. 4, but the wavelength frequency is even more pronounced and of larger amplitude in Fig. 6. The soil vibrations show the presence of the Scholte wave. In the first 20 m, interferences of multiple soil waves are visible, while from 30 m onwards, the Scholte wave at the main driving frequency is clearly visible. Still, this secondary noise path does not affect the fluid pressures visually due to the presence of larger amplitude body waves in the seawater.

The sound pressure levels at two locations shown in Fig. 7 confirm the dominant levels at 150 Hz. Both cases show strong sensitivity to the resonant frequencies of the system. The sound pressure levels induced by the periodic force are significantly larger at almost all frequencies at both locations. The presented case study confirms the hypothesis that the energy in superharmonics is caused by hammer excitation while the non-linear pile–soil interaction plays a secondary role. However, research is required to determine whether the same holds in other conditions, such as variations in hammer characteristics, soil profiles, and pile dimensions.

At the primary driving frequency, the contribution of the Scholte wave to the noise field is observed just above the seabed. Contrary to the periodic force, the case of a single harmonic excitation has the largest noise levels above the seabed at the primary driving frequency. At $z = 4$ m and $r = 100$ m, the Scholte waves are not observed since the waves exponentially decay with depth and minimally affect the upper part of the fluid column. Since body waves cannot travel in the present geometry below the cut-off frequency of the fluid layer (≈ 50 Hz), sound pressure levels are minimal at the main driving frequency away from the pile.

3.3. Comparison with limit cases

The performance of the proposed model is evaluated by comparing it to two linear limit cases of the friction law to assess its added benefits. The first case assumes perfect contact (PC) between the pile and soil, the traditional approach for modelling the

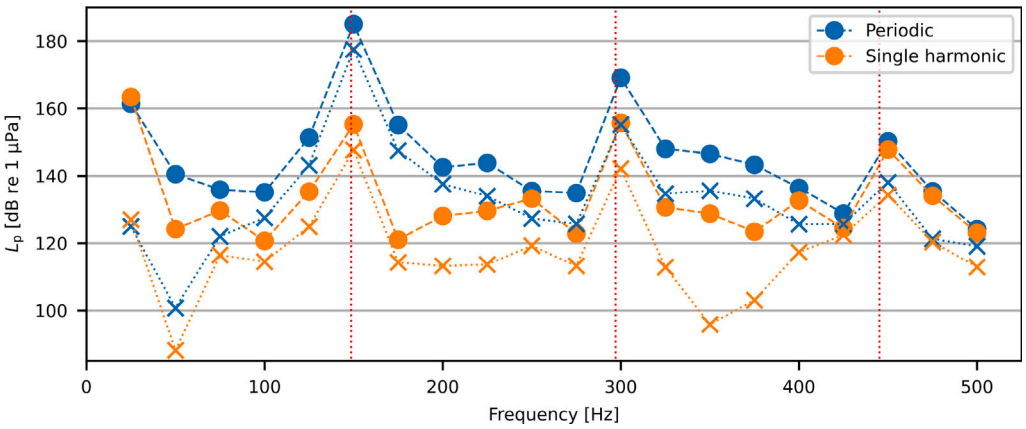

Fig. 7. Sound pressure levels at $r = 25$ m and $z = 7$ m (dashed lines with circle markers) and at $r = 100$ m and $z = 4$ m (dotted lines with crosses) induced by the periodic and single harmonic force, and at a driving depth of $z_2 = 14$ m. The red dotted vertical lines represent the pile's first three in-vacuo natural frequencies.

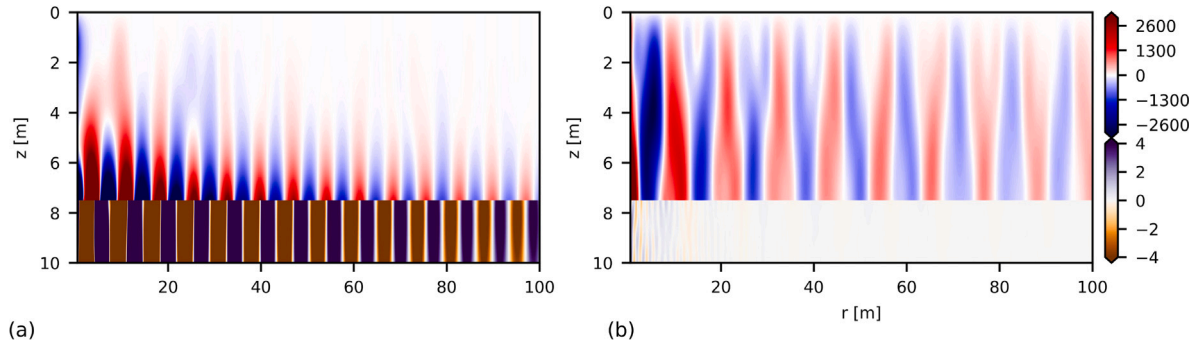

Fig. 8. (a) and (b) show the underwater pressure and seabed vibrations in time at a driving depth of $z_2 = 14$ m for the periodic force, and the case of perfect contact (PC) and no friction (NF), respectively. The blue–red scale shows the fluid pressure in Pa and the yellow–purple scale the vertical soil velocity in $\mathrm{mm\,s^{-1}}$. (For interpretation of the references to color in this figure legend, the reader is referred to the web version of this article.)

interaction between pile and soil in impact pile driving models. The PC case is obtained by replacing the interface conditions, Eqs. (12) and (13) by:

$$u_{\mathrm{p,z}}(z) = u_{\mathrm{s,z}}(r_{\mathrm{p}}, z) \qquad z_1 < z < z_2 \tag{23}$$

$$F_{\mathrm{p,z}}(z) = -\sigma_{\mathrm{s,rz}}(r_{\mathrm{p}}^{+}, z) + \sigma_{\mathrm{s,rz}}(r_{\mathrm{p}}^{-}, z) \qquad z_1 < z < z_2 \tag{24}$$

Second, the assumption of no friction (NF) is made; this is obtained by modifying Eqs. (12) and (13) and setting $F_{\mathrm{Fr}}(z) = 0$. Therefore, the pile and surrounding media are coupled only in the radial direction. Both limit cases are compared to the case with the driveability analysis (DA), i.e. the proposed method.

Due to the linear characteristics when the excitation is harmonic, i.e. at $f = 25$ Hz, both PC and NF models respond to that same frequency because no energy redistributes to higher harmonics. The PC case returns 160, 157 and 155 dB re 1 µPa and the NF case 104, 109 and 114 dB re 1 µPa at $r = 50$ m and $z = 4$ m for the three driving depths of 12, 14 and 16 m, respectively, as presented in Fig. 5. The PC model provides an upper bound for the noise levels at 25 Hz due to the strong presence of the Scholte wave. Contrarily, little noise is produced in the NF case at this low frequency. The pile only interacts with the fluid and soil in the radial direction, and at 25 Hz, no fluid body waves are generated because the driving frequency is below the cut-off frequency of the fluid layer.

Fig. 8 shows fluid pressure and vertical soil velocity excited with the periodic force for the PC and NF cases. The pressure fields significantly differ from those shown in Fig. 6. The body waves at 150 Hz are not observed as strongly in the PC case compared to the proposed method. The NF case shows a wavefield with wavelengths similar to those of the proposed method, though the amplitude of the pressure waves is reduced, and no seabed vibrations are observed. The NF case underestimates the pressure around the seabed and the seabed vibrations. This is the consequence of neglecting all frictional soil forces.

On the contrary, the Scholte interface waves govern the pressure field in the PC case, carrying energy along the seabed–water interface. This is easily observed since the wavelength in soil and fluid matches the wavelength of the Scholte wave at the driving frequency. In the PC case, the vertical velocity of the soil is significantly larger than in other cases; thus, it can be concluded that

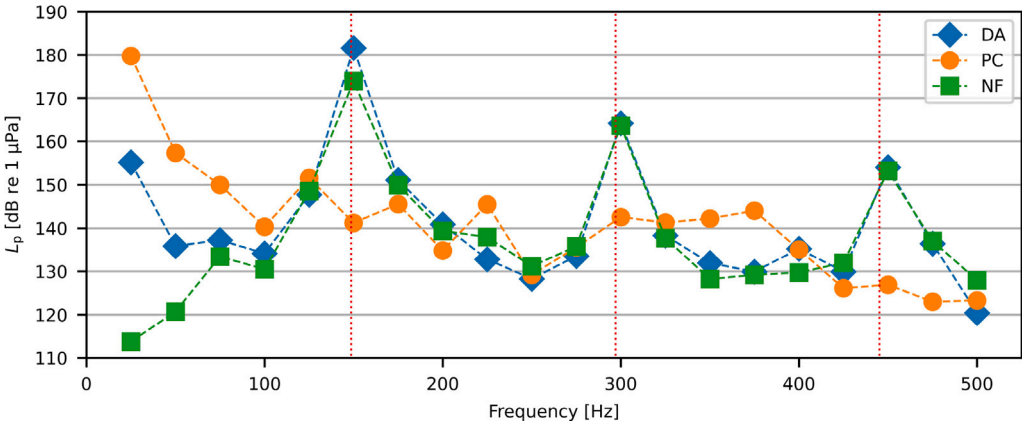

Fig. 9. Sound pressure levels for the three cases at $r = 50$ m and $z = 7$ m and for a driving depth $z_2 = 14$ m.

the PC case overestimates the amplitude of the Scholte wave when the pile and soil are in the sliding mode, which is expected due to the perfect contact of the soil with the pile [21]. This conclusion does not hold when the pile and soil are in sticking mode, i.e., no slip.

Fig. 9 presents the sound pressure levels of the three cases half a metre above the seabed. Except at the low frequencies, the DA case's sound pressure levels show a similar trend to the NF case. However, sound pressure levels deviate by several decibels at some frequencies. Depending on the phase between the superharmonics of the periodic force and the frictional response, friction can dampen or amplify the pile and soil vibrations and, consequently, the fluid pressure levels.

At 150 Hz, the DA case predicts ~ seven dB more than the NF case. Since decibels represent the pressure on a logarithmic scale, fluid pressures and pile vibrations are of different magnitudes. This can only be explained by the friction, which acts as a source at this frequency, exciting the pile vibrations instead of dampening them. This phenomenon is universal and was observed at varying driving depths and excitation frequencies in more cases. The system is susceptible to the dynamic interaction of the components. This observation is consistent with Coulomb friction responding to the sign of the relative pile–soil velocity; thus, the friction changes sign based on the dominant frequency, i.e. the primary driving frequency. Additionally, due to its non-linear characteristics, Coulomb friction distributes energy from the driving frequency to higher harmonics. Consequently, the primary damping mechanism of the pile vibrations at all frequencies except the primary driving frequency is in the radial direction, as in the NF case. The damping obtained is relatively low compared to the PC case, while the radial vibrations of the pile are much smaller in magnitude than the vertical vibrations.

On the other hand, the DA case shows the frequency contribution of the Scholte wave at the 25 Hz that is missing in the NF case, but the effect of the Scholte wave is reduced compared to the PC case. Combining a driveability model with a noise prediction analysis provides results that reasonably close the gap between the two extreme models. Still, an indication of the system resonances at higher harmonics might be possible based on the case of no friction, and an upper bound of the Scholte wave can be deduced from the PC case. It should be considered that the presented case assumes only the state of continuous smooth driving, i.e. no refusal.

3.4. Sensitivity to the driving frequency

The previous analysis clearly shows that the emitted noise field amplifies around the system's resonant frequencies, which, in the case of loose pile–soil coupling along the vertical coordinate, are close to the natural frequencies of the in-vacuo pile. In the examined case, the superharmonics of the periodic force trigger these resonant frequencies. In practice, the driving frequency is adjustable and, thus, an important instrument in reducing noise emissions. This section reduces the primary driving frequency, f_0, from 25 to 23 Hz. The Fourier coefficients c_n do not alter; thus, the force amplitude remains unchanged. First, the effect on driveability must be examined to justify that the change in frequency does not affect driveability. Fig. 10 shows comparable penetration rates for driving at these frequencies which justifies further the detailed acoustic analysis.

The sound pressure levels in the frequency domain vary greatly in both cases, as shown in Fig. 11. The peak in the spectrum of the pressure field at 150 Hz has reduced significantly with the slight reduction of the driving frequency at 23 Hz because the superharmonics are further away from the resonant frequency. The neighbouring superharmonics at 138 and 161 Hz do not resonate as in the case of driving at 25 Hz. The noise radiation around the second and third natural frequencies of the pile is of more comparable amplitude for the two cases. Last, the amplitude of the Scholte wave seems unaffected since equivalent sound pressure levels are predicted at the driving frequency.

Another widely used indicator of the emitted noise is the sound exposure level. The sound exposure levels are found by time-integration of the squared sound pressure [38]:

$$L_E = 10\log\left(\frac{E_p}{E_{ref}}\right), \quad E_p = \int_{t_1}^{t_2} p^2 \mathrm{d}t \tag{25}$$

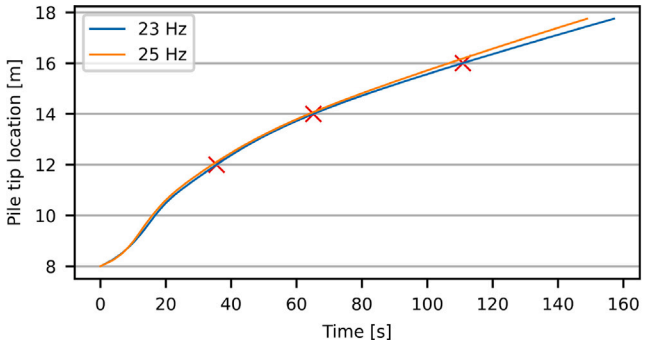

Fig. 10. Pile penetration versus time at 23 and 25 Hz. The red crosses indicate the driving depths at which the noise emission is evaluated.

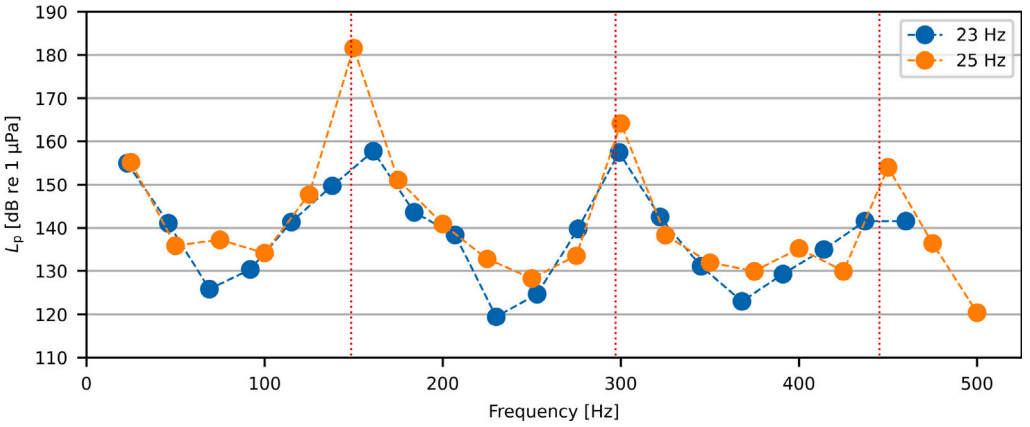

Fig. 11. Comparison of sound pressure levels at $r = 50$ m and $z = 7$ m.

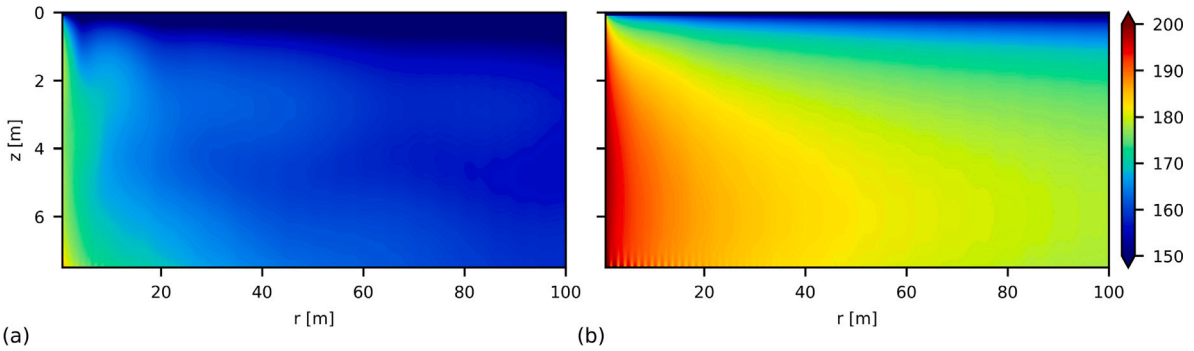

Fig. 12. (a) and (b) show the sound exposure levels, driving with a primary driving frequency of 23 and 25 Hz, respectively, at 14 m driving depth. SELs are given in dB re 1 µPa. (For interpretation of the references to color in this figure legend, the reader is referred to the web version of this article.)

with the reference value for the underwater sound pressure $E_{\text{ref}} = 1\ \mu\text{Pa}^2$ s.

Fig. 12 shows significant differences in the sound exposure levels between the two cases of different driving frequencies. The sound exposure levels differ as much as 20 dB at $r = 100$ m due to the reduced noise emission around 150 Hz. Next to the amplitude, the spatial distribution of the noise also differs. In Fig. 12a, it is observed that the acoustic field is excited by the second in-vacuo mode of the pile. This pile mode has zero radial displacements at the centre of the pile. This corresponds to a driving depth of 14 m with a depth of 5.3 m. Both at the pile's surface and further away from it, the noise levels are significantly lower at this particular depth. Figs. 11 and 12 confirm that the noise levels are sensitive to excitation around the resonant frequency of the immersed structure. This noise reduction mechanism at the source shows high potential in vibratory installation but requires a combined study to optimise pile driveability and noise emission. None of the existing linear models can predict this complex behaviour to optimise the installation both from a driveability and noise emission perspective.

Table 2
Parameters for the large diameter monopile case study [37].

Parameter		Unit	Parameter		Unit
Sea surface depth [z_1]	0	m	Fluid wave speed [c_f]	1500	$m\,s^{-1}$
Seabed depth [z_2]	40	m	Fluid density [ρ_f]	1000	$kg\,m^{-3}$
Pile length [L_p]	76.9	m	Compression wave speed soil [c_L]	1979	$m\,s^{-1}$
Pile thickness [t_p]	9	cm	Shear wave speed soil [c_T]	349	$m\,s^{-1}$
Pile radius [r_p]	4	m	Soil density [ρ_s]	1950	$kg\,m^{-3}$
Pile Poisson's ratio [ν_p]	0.30	–	Compressional wave attenuation [α_L]	0.27	dB/λ
Pile Young's modulus [E_p]	210	GPa	Shear wave attenuation [α_T]	1.09	dB/λ
Pile density [ρ_p]	7850	$kg\,m^{-3}$	Cone tip resistance [q_c]	18	MPa
Structural damping [η_p]	0.001	–			

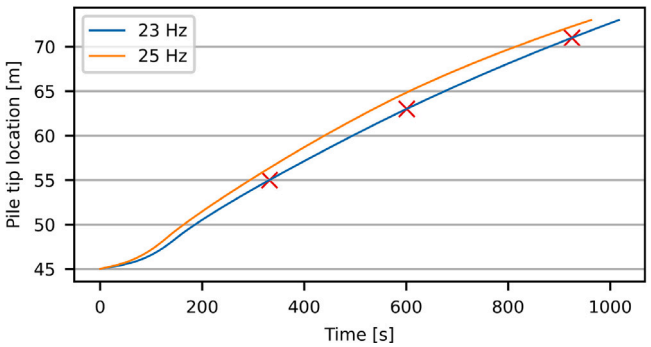

Fig. 13. Penetration of large-diameter monopile versus time with driving frequencies $f_0 = 23$ and 25 Hz. The red crosses indicate driving depths at which the noise emission is evaluated.

4. Underwater noise field of a large-diameter monopile

The trend towards larger monopile foundations for offshore wind turbines is notable. This section delves into the case of an 8-metre diameter monopile installed through impact piling in the German North Sea, as detailed by [37]. The hypothetical scenario is investigated in which a vibratory installation tool drives the same foundation pile into the soil. This section contains an analysis that compares sound levels with limit case elastic models, evaluates the influence of driving depth on sound emission, and explores the sensitivity of sound emission to a shift in primary driving frequency. The relevant geometric and material properties are outlined in Table 2. Two cases considered run with a periodic force atop the large-diameter monopile with a primary driving frequency of $f_0 = 23$ and 25 Hz. The spectral distribution of the force amplitude is the same as in the small diameter case. The amplitudes are increased by 30 to ensure a continuous and sensible penetration rate of approximately three $cm\,s^{-1}$, illustrated in Fig. 13.

4.1. Comparison with limit cases

Fig. 14 compares the sound pressure levels 5 m above the seabed at 50 m radius for the cases of DA, PC and NF. Besides the sound pressure levels, vertical red dashed lines indicate the pile's first five axisymmetric in-vacuo eigenfrequencies and the blue dotted line indicates the ring frequency. The first few in-vacuo eigenfrequencies of the large-diameter monopile are notably lower than those of smaller-diameter piles, approaching the primary driving frequency. Consequently, tuning the driving frequency to avoid interference with the sensitive frequency response of the coupled system becomes quite challenging. The graphical representation underscores the interference of the second superharmonic at 69 Hz with the second resonance frequency of the in-vacuo pile (67 Hz), resulting in amplified sound levels. This resonance behaviour aligns with observations in the smaller-diameter pile scenario, where resonant frequencies minimally deviate from the eigenfrequencies of the in-vacuo pile. A similar, though less pronounced, interference is evident at 145 Hz. On the contrary, the monolithic connection makes all resonances less prominent in the PC case.

The modal density is highest around the ring frequency at 216 Hz. However, waves excited around this frequency do not typically generate noise because the energy barely propagates through the pile due to the low vertical group velocity. An exception exists when the top of the pile is submerged. This observation persists across all three cases presented in Fig. 14.

Similar to the small-diameter pile scenario, the NF approximation exhibits analogous trends to the proposed method across frequencies, except at the driving frequency. Differences in sound pressure levels between NF and DA cases are minor, suggesting diminished prominence of friction-induced vibrations relative to excitation by the energy introduced in the superharmonics by the hammer. At the driving frequency, PC and NF approximations exhibit discrepancies in sound levels compared to the DA case, attributed to monolithic coupling and strong excitation of surface waves along the seabed in the PC case and the lack of frictional forces in the NF case.

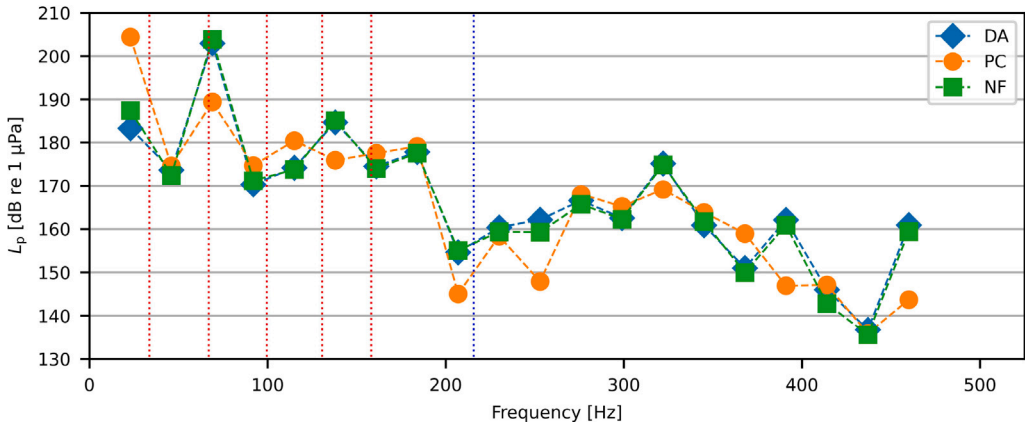

Fig. 14. Sound pressure levels compared to the cases of perfect contact and no friction at $f_0 = 23$ Hz, $r = 50$ m, $z = 35$ m and $z_2 = 63$ m. Vertical red dotted lines indicate the first 5 in-vacuo eigenfrequencies of the pile, and the blue dotted line indicates the ring frequency.

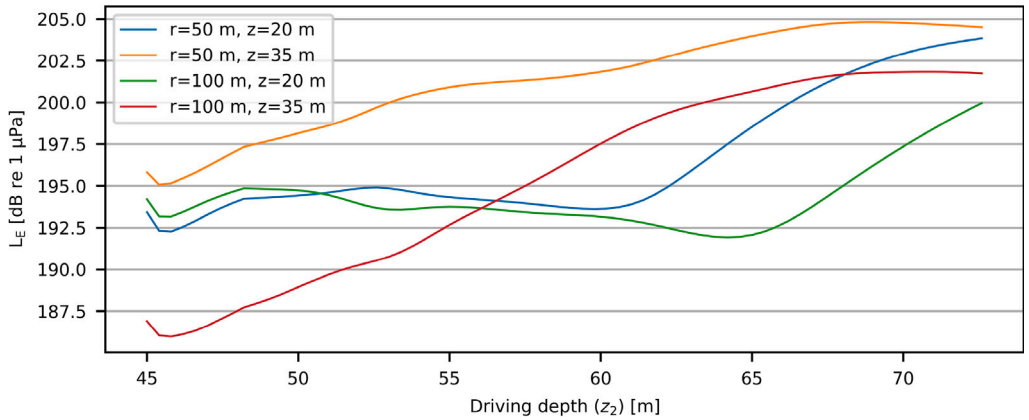

Fig. 15. Sound exposure levels during driving with a driving force of 23 Hz at four observation points in the fluid.

4.2. Effect of driving depth

As the driving depth proceeds, several factors influence the dynamic response and sound levels. These include added mass, damping, and stiffness due to soil and fluid in the radial direction, frictional pile–soil resistance, friction degradation, and the location with modal nodes with no radial displacements. Consequently, predicting the influence of driving depth on dynamic response and sound levels necessitates detailed analysis.

Fig. 15 illustrates substantial sound exposure level variations based on driving depth. Changes in SEL exhibit distinct patterns depending on the observer's location. Notably, an increase in SEL is observed after 60 metres of driving when the observer point is halfway through the fluid column. At the same time, a gradual increase with a slight decrease upon reaching full penetration is evident just above the seabed. These trends contrast the decreasing sound levels with driving depth observed in small-diameter monopiles.

The snapshots in time presented in Fig. 16 offer insight into the fluid pressure and sound exposure level changing in the entire fluid column. The dominance of the second flexural mode of the pile in noise generation is evident. The second in-vacuo pile mode has a node in the middle of the pile, located at $z = 16.55$, 24.55 and 32.55 m for the three considered driving depths, respectively. At the node, the mode has no radial displacement. These depths are visually identified in the pressure field since pressures here are significantly lower. Also, the sound exposure levels presented in Fig. 16b, clearly indicate the locations of the modal node. At almost complete penetration, the place where radial deformations of the second mode are maximal, i.e. a quarter of a pile length, is in the middle of the fluid column, leading to the highest noise levels in the field.

Additionally, waves with shorter wavelengths near the pile surface are observed, belonging to the evanescent field, which does not propagate radially. It should be noted that sound levels do not depend solely on the generated pressure field but also on the

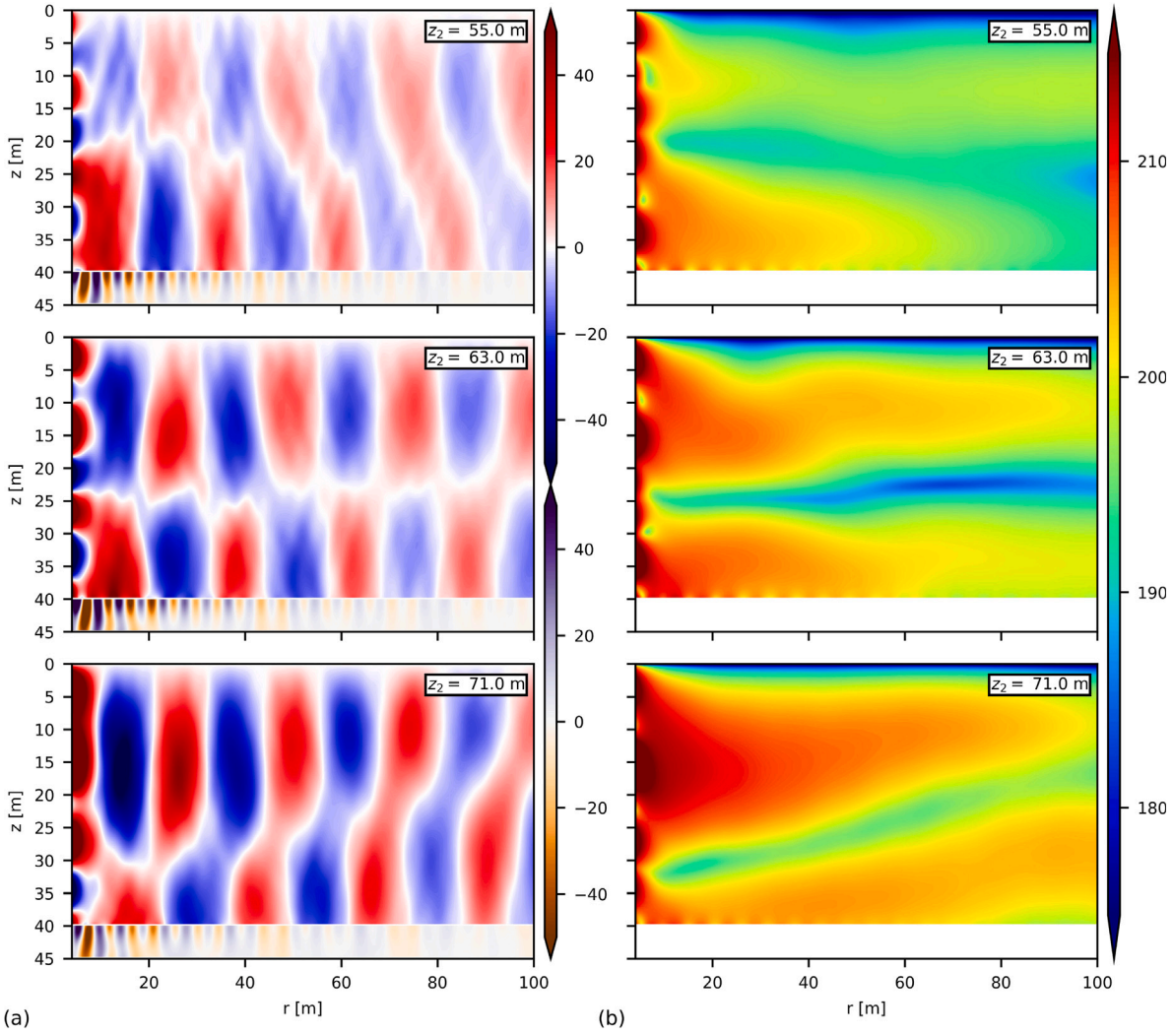

Fig. 16. (a) Snapshots in time of the pressure levels and vertical seabed velocity at three driving depths, in kPa and mm s^{-1}, respectively and (b) the sound exposure levels in dB re 1 μPa. (For interpretation of the references to color in this figure legend, the reader is referred to the web version of this article.)

energy that can propagate away from the pile surface. Finally, Scholte waves are generated at the primary driving frequency but have a negligible impact on the sound exposure levels, except for positions on the seabed surface or at a short distance from the pile's surface. The frequency of the Scholte wave is identified by its wavelength of about 14 m, examining the vertical soil velocity. Based on the above observations, a singular noise prediction based on a single driving depth is deemed inadequate for determining the highest expected sound levels during vibratory pile driving installations.

4.3. Sensitivity to driving frequency

Slight deviations in the excitation frequency of the hammer significantly influence the spectral noise levels for the large-diameter monopile, shown in Fig. 17, akin to the scenario with the small-diameter pile. Interference between the superharmonics at 25 Hz and higher harmonics of the pile occurs. However, amplification of sound levels is not observed, i.e. the sound levels show no resonance around the second in-vacuo frequency of the pile when driving at 25 Hz. Multiple attributes contribute to the presence of resonance, e.g., the location of the pile nodes, resonance frequencies being shifted or eliminated due to added mass, damping or stiffness of fluid and soil, and sound not propagating because evanescent modes instead of propagating modes are excited. Kaynia et al. [27] have reported similar observations in vibro-driving of monopiles, where strong frequency-dependence of dynamic stiffness was associated with the dynamic behaviour of the inner soil column. The complex and non-linear nature of the system suggests that a detailed analysis is imperative to incorporate sensitivity to driving frequencies in noise predictions.

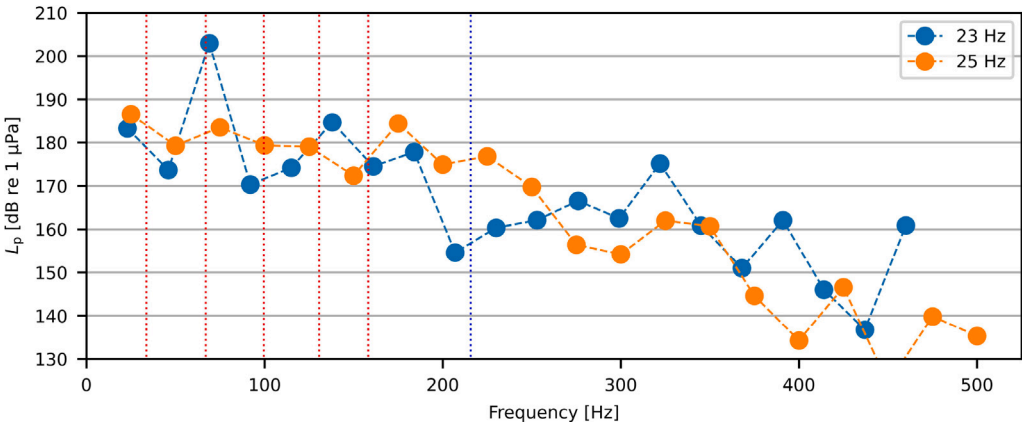

Fig. 17. Sound pressure levels driving at 23 and 25 Hz at $r = 50$ m, $z = 35$ m and $z_2 = 63$ m. Vertical red dotted lines indicate the first five in-vacuo eigenfrequencies of the pile, and the blue dotted line indicates the ring frequency.

5. Conclusions

The paper introduces a novel methodology for underwater noise predictions during vibratory pile driving. A non-linear driveability model is used to obtain realistic interface friction forces as input for a noise prediction model. The paper demonstrates the importance of incorporating a driveability analysis, finding significant differences from traditional models that assume perfect contact between the pile and soil. The authors contend that the proposed model yields more realistic results under the assumption of smooth driving without refusal compared to traditional linear models that assume perfect contact used in impact piling. The results show a clear deviation in pressure levels and seabed vibrations between the linear and presented methods at the driving frequency and superharmonics. A few significant findings are discussed below:

- The primary source of noise generation is the radial vibrations of the pile. These are amplified around the resonant frequencies of the coupled system, which are close to the in-vacuo frequencies of the pile when loosely coupled. The coexistence of the resonant frequencies and superharmonics of the force can amplify the sound pressure levels. Thus, even a small shift in driving frequency can significantly decrease the noise generated, a promising finding from a practical perspective.
- The noise field is found to be highly sensitive to the change in the system dynamics during penetration of both small and large monopiles. The driving depth of the pile significantly affects the dynamic response as various conditions alter during driving. Based on the cases presented, it is unclear what the critical driving depth is. Therefore, noise predictions are advised throughout the driving process in vibratory pile driving.
- The Coulomb friction responds mainly to the driving frequency and shifts energy to higher harmonics. Depending on the phase, this can either excite or dampen the pile vibrations. A reasonable first approximation of the noise field is obtained by assuming no friction between the pile and soil. However, seabed vibrations cannot be predicted through the no-friction assumption, and pile vibrations may be inaccurate in certain soil configurations.
- Noise predictions during vibro-driving are heavily influenced by the superharmonics generated by the hammer. These superharmonics, resulting from the periodic signal of the hammer, appear to have greater significance than vibrations induced by friction. However, several factors influence the force exerted by the vibro hammer, including driving frequency, hammer type, pile size, soil characteristics, pile-hammer connection, and line load. The amount of energy in the superharmonics will significantly affect the predicted noise levels. Therefore, future research incorporating extensive experimental data is necessary to establish generalised conclusions.
- Efforts to optimise the vibro hammer to minimise the generation of superharmonics can positively reduce noise levels. However, even with single-harmonic excitation, the friction causes energy to shift towards higher harmonics. Acknowledging that friction forces are highly non-linear is essential. Consequently, friction forces do not scale linearly with excitation or frequency shifts, resulting in changing underwater noise levels that are difficult to predict without detailed analysis.

We conclude that the dynamic interaction between all components in the system plays a crucial role in predicting underwater noise levels during vibratory pile driving. The system is primarily sensitive to the driving frequency and its superharmonics, which may strongly interfere with the system's resonant frequencies. Hence, a detailed analysis, including an accurate description of the pile–soil interface, is essential to predict the underwater noise field and seabed vibrations accurately.

CRediT authorship contribution statement

Timo Molenkamp: Conceptualization, Formal analysis, Investigation, Methodology, Validation, Visualization, Writing – original draft, Writing – review & editing. **Athanasios Tsetas:** Formal analysis, Methodology, Validation, Writing – review & editing.

Apostolos Tsouvalas: Supervision, Writing – review & editing. **Andrei Metrikine:** Funding acquisition, Supervision, Writing – review & editing.

Declaration of competing interest

The authors declare that they have no known competing financial interests or personal relationships that could have appeared to influence the work reported in this paper.

Data availability

No data was used for the research described in the article.

Acknowledgments

This paper is associated with the GDP project in the framework of the GROW joint research program. Funding from *Topsector Energiesubsidie van het Ministerie van Economische Zaken*, The Netherlands under grant number TEHE117100 and financial/technical support from the following partners is gratefully acknowledged: Royal Boskalis Westminster N.V., The Netherlands, CAPE Holland B.V., The Netherlands, Deltares, The Netherlands, Delft Offshore Turbine B.V., Delft University of Technology, The Netherlands, ECN, The Netherlands, Eneco Wind B.V., The Netherlands, IHC IQIP B.V., The Netherlands, RWE Offshore Wind Netherlands B.V., The Netherlands, SHL Offshore Contractors B.V., The Netherlands, Shell Global Solutions International B.V., Sif Netherlands B.V., The Netherlands, TNO, The Netherlands, and Van Oord Offshore Wind Projects B.V, The Netherlands.

References

[1] European Commission, Communication from the Commission to the European Parliament, the Council, the European Economic and Social Committee and the Committee of the Regions: An EU Strategy to harness the potential of offshore renewable energy for a climate neutral future, in: COM(2020) 741 Final, Technical Report, 2020, p. 27.

[2] A. Memija, First XXL monopile installed at Arcadis ost 1, 2022, URL: https://www.offshorewind.biz/2022/06/09/first-xxl-monopile-installed-at-arcadis-ost-1/.

[3] P. Madsen, M. Wahlberg, J. Tougaard, K. Lucke, P. Tyack, Wind turbine underwater noise and marine mammals: implications of current knowledge and data needs, Mar. Ecol. Prog. Ser. 309 (Tyack 1998) (2006) 279–295, http://dx.doi.org/10.3354/meps309279, URL: http://www.int-res.com/abstracts/meps/v309/p279-295/.

[4] P.H. Dahl, P.G. Reinhall, A.N. Popper, M.C. Hastings, M.A. Ainslie, Underwater sound from pile driving, what is it and why does it matter, J. Acoust. Soc. Am. 135 (4) (2014) 2312, http://dx.doi.org/10.1121/1.4877620, URL: http://asa.scitation.org/doi/10.1121/1.4877620 http://acousticstoday.org/wp-content/uploads/2015/06/The-Underwater-Sound-Field-from-Impact-Pile-Driving-and-Its-Potential-Effects-on-Marine-Life-Peter-H.-Dahl-Christ-A.-F.-de-Jong-and-Arthur-N.-Popper.pdf.

[5] B.L. Southall, J.J. Finneran, C. Reichmuth, P.E. Nachtigall, D.R. Ketten, A.E. Bowles, W.T. Ellison, D.P. Nowacek, P.L. Tyack, Marine Mammal Noise Exposure Criteria: Updated Scientific Recommendations for Residual Hearing Effects, Aquatic Mammals 45 (2) (2019) 125–232, http://dx.doi.org/10.1578/AM.45.2.2019.125, URL: https://www.aquaticmammalsjournal.org/index.php?option=com{_}content&view=article&id=1886:marine-mammal-noise-exposure-criteria-updated-scientific-recommendations-for-residual-hearing-effects&catid=174&Itemid=326.

[6] A. Benhemma-Le Gall, I.M. Graham, N.D. Merchant, P.M. Thompson, Broad-scale responses of harbor porpoises to pile-driving and vessel activities during offshore windfarm construction, Front. Mar. Sci. 8 (July) (2021) 1–18, http://dx.doi.org/10.3389/fmars.2021.664724, URL: https://www.frontiersin.org/articles/10.3389/fmars.2021.664724/full.

[7] P.G. Reinhall, P.H. Dahl, Underwater Mach wave radiation from impact pile driving: Theory and observation, J. Acoust. Soc. Am. 130 (3) (2011) 1209–1216, http://dx.doi.org/10.1121/1.3614540, URL: http://asa.scitation.org/doi/10.1121/1.3614540.

[8] T. Lippert, S. Lippert, Modelling of pile driving noise by means of wavenumber integration, Acoust. Aust. 40 (3) (2012) 178–182.

[9] M. Zampolli, M.J.J. Nijhof, C.A.F. de Jong, M.A. Ainslie, E.H.W. Jansen, B.A.J. Quesson, Validation of finite element computations for the quantitative prediction of underwater noise from impact pile driving, J. Acoust. Soc. Am. 133 (1) (2013) 72–81, http://dx.doi.org/10.1121/1.4768886, URL: http://asa.scitation.org/doi/10.1121/1.4768886.

[10] A. Tsouvalas, A.V. Metrikine, A semi-analytical model for the prediction of underwater noise from offshore pile driving, J. Sound Vib. 332 (13) (2013) 3232–3257, http://dx.doi.org/10.1016/j.jsv.2013.01.026.

[11] Q. Deng, W. Jiang, M. Tan, J.T. Xing, Modeling of offshore pile driving noise using a semi-analytical variational formulation, Appl. Acoust. 104 (2016) 85–100, http://dx.doi.org/10.1016/j.apacoust.2015.11.002.

[12] A. Tsouvalas, A.V. Metrikine, A three-dimensional vibroacoustic model for the prediction of underwater noise from offshore pile driving, J. Sound Vib. 333 (8) (2014) 2283–2311, http://dx.doi.org/10.1016/j.jsv.2013.11.045, URL: http://link.springer.com/10.1007/978-3-642-40371-2{_}38.

[13] M.B. Fricke, R. Rolfes, Towards a complete physically based forecast model for underwater noise related to impact pile driving, J. Acoust. Soc. Am. 137 (3) (2015) 1564–1575, http://dx.doi.org/10.1121/1.4908241, URL: http://asa.scitation.org/doi/10.1121/1.4908241.

[14] R. He, Y. Xiang, Z. Guo, A Poroelastic Model for Near-Field Underwater Noise Caused by Offshore Monopile Driving, J. Sound Vib. (2023) 117878, http://dx.doi.org/10.1016/j.jsv.2023.117878.

[15] A. Tsouvalas, A.V. Metrikine, Noise reduction by the application of an air-bubble curtain in offshore pile driving, J. Sound Vib. 371 (2016) 150–170, http://dx.doi.org/10.1016/j.jsv.2016.02.025.

[16] Y. Peng, A. Tsouvalas, T. Stampoultzoglou, A.V. Metrikine, Study of the Sound Escape with the Use of an Air Bubble Curtain in Offshore Pile Driving, J. Mar. Sci. Eng. 9 (2) (2021) 232, http://dx.doi.org/10.3390/jmse9020232, URL: https://www.mdpi.com/2077-1312/9/2/232.

[17] N. Moscoso del Prado Mazza, A. Holeyman, Frequency-penetration response spectrum on vibratory amplitude matching of monopiles, ISBN: 978-0-8031-7667-6, 2019, pp. 468–492, http://dx.doi.org/10.1520/STP161120170243.

[18] A. Tsetas, A. Tsouvalas, S.S. Gómez, F. Pisanò, E. Kementzetzidis, T. Molenkamp, A.S. Elkadi, A.V. Metrikine, Gentle Driving of Piles (GDP) at a sandy site combining axial and torsional vibrations: Part I - installation tests, Ocean Eng. 270 (April 2022) (2023) 113453, http://dx.doi.org/10.1016/j.oceaneng.2022.113453.

[19] A. Tsouvalas, A.V. Metrikine, Structure-borne wave radiation by impact and vibratory piling in offshore installations: From sound prediction to auditory damage, J. Mar. Sci. Eng. 4 (3) (2016) 44, http://dx.doi.org/10.3390/jmse4030044, URL: http://www.mdpi.com/2077-1312/4/3/44.
[20] P.H. Dahl, D.R. Dall'Osto, D.M. Farrell, The underwater sound field from vibratory pile driving, J. Acoust. Soc. Am. 137 (6) (2015) 3544–3554, http://dx.doi.org/10.1121/1.4921288, URL: http://asa.scitation.org/doi/10.1121/1.4921288.
[21] T. Molenkamp, A. Tsouvalas, A. Metrikine, The influence of contact relaxation on underwater noise emission and seabed vibrations due to offshore vibratory pile installation, Front. Mar. Sci. 10 (March) (2023) 357, http://dx.doi.org/10.3389/FMARS.2023.1118286, URL: https://www.frontiersin.org/articles/10.3389/fmars.2023.1118286/full.
[22] A. Tsetas, A. Tsouvalas, A.V. Metrikine, A non-linear three-dimensional pile–soil model for vibratory pile installation in layered media, Int. J. Solids Struct. 269 (2023) 112202, http://dx.doi.org/10.1016/j.ijsolstr.2023.112202.
[23] A.W. Leissa, Vibration of Shells, Technical Report, Scientific and Technical Information Office National Aeronautics and Space Administration, Washington, D.C., 1973, p. 428.
[24] F.B. Jensen, W.A. Kuperman, M.B. Porter, H. Schmidt, in: W.M. Hartmann (Ed.), Computational Ocean Acoustics, seccond ed., Springer New York, New York, NY, 2011, p. 794, http://dx.doi.org/10.1007/978-1-4419-8678-8, URL: http://link.springer.com/10.1007/978-1-4419-8678-8.
[25] R. Salgado, D. Loukidis, G. Abou-Jaoude, Y. Zhang, The role of soil stiffness non-linearity in 1D pile driving simulations, Géotechnique 65 (3) (2015) 169–187.
[26] R. Buckley, Y.M. Chen, B. Sheil, S. Suryasentana, D. Xu, J. Doherty, M. Randolph, Bayesian optimization for CPT-based prediction of impact pile drivability, J. Geotech. Geoenviron. Eng. 149 (11) (2023) 04023100.
[27] A.M. Kaynia, J. Hebig, T. Pein, Y. Shin, Numerical model for dynamic installation of large diameter monopiles, Soil Dyn. Earthq. Eng. 161 (2022) 107393.
[28] E. Kausel, R. Peek, Dynamic loads in the interior of a layered stratum: an explicit solution, Bull. Seismol. Soc. Am. 72 (5) (1982) 1459–1481.
[29] E. Kausel, J.M. de Oliveira Barbosa, PMLs: A direct approach, Internat. J. Numer. Methods Engrg. 90 (3) (2012) 343–352.
[30] J.M. de Oliveira Barbosa, J. Park, E. Kausel, Perfectly matched layers in the thin layer method, Comput. Methods Appl. Mech. Engrg. 217 (2012) 262–274.
[31] S. Moriyasu, S. Kobayashi, T. Matsumoto, Experimental study on friction fatigue of vibratory driven piles by in situ model tests, Soils Found. 58 (4) (2018) 853–865.
[32] M. Krack, L. Panning-von Scheidt, J. Wallaschek, A high-order harmonic balance method for systems with distinct states, J. Sound Vib. 332 (21) (2013) 5476–5488.
[33] S. Zhou, J. Cao, D.J. Inman, J. Lin, D. Li, Harmonic balance analysis of nonlinear tristable energy harvesters for performance enhancement, J. Sound Vib. 373 (2016) 223–235.
[34] F. Fontanela, A. Grolet, L. Salles, N. Hoffmann, Computation of quasi-periodic localised vibrations in nonlinear cyclic and symmetric structures using harmonic balance methods, J. Sound Vib. 438 (2019) 54–65.
[35] A. Tsetas, A. Tsouvalas, A.V. Metrikine, The mechanics of the gentle driving of piles, Int. J. Solids Struct. 282 (2023) 112466.
[36] A. Tsetas, A Unified Modelling Framework for Vibratory Pile Driving Methods (Ph.D. thesis), Delft University of Technology, 2023.
[37] Y. Peng, A. Tsouvalas, T. Stampoultzoglou, A.V. Metrikine, A fast computational model for near- and far-field noise prediction due to offshore pile driving, J. Acoust. Soc. Am. 149 (3) (2021) 1772–1790, http://dx.doi.org/10.1121/10.0003752, URL: https://asa.scitation.org/doi/10.1121/10.0003752.
[38] ISO, ISO 18405:2017 Underwater Acoustics — Terminology, International Organization for Standardization, 2017, URL: https://www.iso.org/standard/62406.html.